Journal of Electronic Materials (2023) 52:1493–1506
https://doi.org/10.1007/s11664-022-10113-y

ORIGINAL RESEARCH ARTICLE

Study on the Crystallization Behavior of Sb_2Te Thin Films for Phase-Change Memory Applications

Lei Kang[1] · Haiqing Yin[2,3] · Leng Chen[1]

Received: 23 September 2022 / Accepted: 17 November 2022 / Published online: 12 December 2022
© The Minerals, Metals & Materials Society 2022

Abstract
Sb_2Te thin films were deposited on SiO_2/Si (100) substrates by magnetron sputtering. We investigated the crystallization behavior of Sb_2Te thin films for phase-change memory applications. The experimental results show that the optical reflectivity is increased by more than 30% before and after crystallization. The resistance is decreased at least 10^2 orders of magnitude in the crystallization process, which suggests the application potential of Sb_2Te thin film as optoelectronic storage material. The computational results show that the local crystallization activation energy is 1.72 eV and the crystal growth velocity is 4.96 m s^{-1}, confirming the strong crystallization tendency of Sb_2Te thin film. We examined the features of amorphous local bonding and found that the local octahedral geometry is the structural origin of optoelectronic contrast and crystallization tendency. Furthermore, the presence of weak Sb-Sb, Sb-Te, and Te-Te bonds and high mobility of Sb atoms facilitate the high-speed and low-activation-energy crystallization. Hence, we suggested that reducing the number of octahedrons and introducing the strong chemical bonds could promote stable optoelectronic memory applications of Sb_2Te thin film.

Keywords Phase-change memory · Sb_2Te · crystallization kinetics · local bonding · optoelectronic switching application

Introduction

Following the pioneering investigation of Ovshinsky,[1] chalcogenide alloys, which can quickly change from an amorphous to a crystalline state at the nanosecond (ns) scale, have attracted the attention of scientists for many years. The striking electrical contrast between disordered and ordered phases has also been confirmed. Thanks to the excellent electrical conversion properties, chalcogenide compounds have been applied for phase-change random access memory (PCRAM). To perform the SET operation, a moderate electric pulse is employed to crystallize the amorphous phase-change memory (PCM) layer. In the RESET process, the crystalline PCM material transforms to the amorphous state under an intensive pulse.[2] Data transfer is largely dependent on the phase transformation of the PCM alloy. Understanding the structural transition behavior is urgently needed.

$Ge_2Sb_2Te_5$ is a prototype PCM material. Many studies have been performed on the crystallization behavior of $Ge_2Sb_2Te_5$. Sutou et al.[3] reported a decrease in the Avrami exponent with increasing crystallinity of $Ge_2Sb_2Te_5$, indicating obvious crystal growth with decreasing nucleation rate. This means that crystallization is a multi-stage process where the properties of the PCM material change as a result. The non-Arrhenius grain growth behavior of $Ge_2Sb_2Te_5$ was confirmed, implying the high-fragility crystallization characteristic.[4] High-fragility crystallization promotes the stability of the amorphous structure at low temperature and rapid crystallization at high temperature, which are critical properties for PCM applications.[5] Therefore, the crystallization behavior of the PCM layer largely determines storage applications. The structural origin of crystallization characteristics is worth exploring. In the umbrella-flip model, sliding Ge atoms induce rapid conversion of Ge-Te bonds, supporting fast crystallization of $Ge_2Sb_2Te_5$,[6] whereas the strong Ge-Te bond in the tetrahedral environment could increase structural rigidity and reduce the tendency for

✉ Leng Chen
lchen@ustb.edu.cn

1 School of Materials Science and Engineering, University of Science and Technology Beijing, Beijing 100083, China

2 Collaborative Innovation Center of Steel Technology, University of Science and Technology Beijing, Beijing 100083, China

3 Beijing Advanced Innovation Center for Materials Genome Engineering, University of Science and Technology Beijing, Beijing 100083, China

crystallization.[7] Akola and Jones[8] ascribed the crystallization of $Ge_2Sb_2Te_5$ to the rearrangement of ABAB (A for Sb/Ge atom, B for Te atom) rings, which implies that the local structural motifs play an important role in the crystallization process. Analysis of crystallization characteristics allows to improve the properties and applications of PCM materials.

Research is continuously improving crystallization characteristics and exploring advanced PCM systems. Sb_2Te, a novel Sb-based PCM material, exhibits rapid phase transition. The conversion time is 20 ns for the Sb_2Te-based PCM device, close to that of the DRAM (< 10 ns).[9] Nevertheless, the data retention temperature (55°C/10 years) limits its application in more challenging scenarios, such as the Internet of Things, neuron computing, and automotive electronic systems, where a minimum retention temperature of 120°C/10 years is required.[10] Faster crystallization and lower amorphous thermal stability imply a higher crystallization trend, limiting the application of Sb_2Te for more stable memory. To improve its performance, extensive studies have been performed on doped Sb_2Te.[11–23] Nonetheless, only a few studies have been conducted on the crystallization characteristics and related physical mechanisms of Sb_2Te itself.[24] A careful examination of the evolution of the microstructure and properties provides direct insight into the crystallization process. Analyzing the crystallization kinetics is useful for understanding the crystallization behavior. Attention should be paid to the amorphous local bonding of Sb_2Te. It is worth exploring the correlation between local structural features and crystallization transition, which is important in advancing the application of Sb_2Te for more stable storage.

Motivated by this topic, we focused on the crystallization behavior of Sb_2Te thin films to explore the application potential for stable storage. First of all, the microstructure and photo-electronic properties were monitored to directly understand the crystallization transition. Then, the crystallization kinetics was studied, where the local crystallization activation energy and crystal growth velocity were calculated to quantitatively describe the crystallization behavior. Next, we linked the crystallization behavior to the amorphous local structure. The chemical bonding and atomic diffusion of the amorphous Sb_2Te thin film were explored experimentally and theoretically. Finally, we made suggestions to adjust the amorphous local bonding of Sb_2Te thin film for more stable optoelectronic memory applications.

Experimental Details

Preparation of the Thin Films

Sb_2Te thin films with 200 nm thickness were deposited on SiO_2/Si (100) wafers by DC magneton sputtering using a single stoichiometric Sb_2Te target. The background pressure was below 10^{-6} kPa. The argon pressure was fixed at 6.6×10^{-4} kPa with a flow rate of 33 sccm. Substrate rotation with a speed of 20 rpm was used to ensure homogeneous deposition. The as-deposited thin film was annealed at 300°C for 30 min under a vacuum atmosphere (< 10^{-6} kPa) to obtain the crystalline state.

Optoelectronic Properties Measurements

The temperature-dependent resistance of the as-deposited thin film was monitored in situ by a four-point probe system with a heating rate of 5°C min^{-1}. The optical reflectivity of the as-deposited and annealed thin films was measured by UV–Vis spectroscopy (Shimadzu UV-2550) at visible wavelengths. The microstructure of the annealed thin film was characterized by electron backscatter diffraction (EBSD) (Oxford Instruments).

Kinetics Analysis

Differential scanning calorimetry (DSC) was employed to record the crystallization process under various heating rates (10°C min^{-1}, 20°C min^{-1}, 30°C min^{-1}, and 40°C min^{-1}) in a high-purity argon protection environment. Sb_2Te thin films of 1000 nm thickness were measured to improve the signal-to-noise ratio of DSC traces. The obtained DSC curves were used to investigate the crystallization kinetics of Sb_2Te thin film.

Structure Characterization

X-ray photoelectron spectroscopy (XPS) was performed to survey the chemical bonding states of the as-deposited thin film. Raman measurement was used to identify the vibration modes in the as-deposited thin film. Theoretical investigations were carried out by means of density functional theory (DFT) using CASTEP.[25] Molecular dynamics (MD) simulation was employed to generate an amorphous Sb_2Te model. The ultrasoft pseudopotentials were used to describe electron–ion interactions. The electronic exchange–correlation energies were described by the generalized gradient approximation based on the Perdew–Burke–Ernzerhof functional.[26] The energy cutoff was chosen to be 230 eV. The k points of $2 \times 2 \times 1$ was set. The NVT ensemble was used. The initial configuration is a Sb_2Te hexagonal supercell with 144 atoms. To ensure reliable computation, the atomic density was set to experimental value (30.5 atoms nm^{-3}).[16] Steps of 3 femtoseconds (fs) were employed. The model was melted at 2000 K for 2000 steps to erase the orderly arrangement of atoms. The molten system was equilibrated at 1200 K for 5000 steps. The model was quenched to 300 K and equilibrated for 10,000 steps to reach an amorphous state.

Results and Discussion

Crystallization Process of Sb_2Te Thin Film

Electrical Resistance Change

The change in thin film resistance with increasing temperature is monitored to understand the crystallization transition in real time. As shown in Fig. 1, a sudden drop in thin film resistance can be observed around 130°C, which is the signature of crystallization. Before crystallization, the thin film resistance reduces slowly with increasing temperature, which may be due to the thermally induced transport.[27] After the phase transition, the thin film resistance is almost unchanged with rising temperature, which implies a stable crystal phase. It is evident that the resistance is reduced at least 10^2 orders of magnitude after crystallization for Sb_2Te thin film, enabling data reading reliability.[18] To discuss the crystallization temperature (T_c) of Sb_2Te thin film, the differential of the R–T curve has been computed (Fig. 1). The T_c is determined as the temperature corresponding to the minimum of the differential curve.[20] The T_c of Sb_2Te thin film, estimated to be ~ 132.9°C, is clearly lower than that of $Ge_2Sb_2Te_5$ (~ 155°C),[15] showing a strong crystallization tendency for amorphous Sb_2Te thin film.

Optical Reflectivity Transition

The optical transition is an important signal of crystallization. As shown in Fig. 2, the reflectivity of the as-deposited and crystalline Sb_2Te thin films are 45% and 63%. The optical reflectivity contrast (C) has been computed by using the following equation:[28]

$$C = 2 \times \left| \frac{R_a - R_c}{R_a + R_c} \right| \times 100\% \quad (1)$$

where R_a and R_c are the reflectance before and after crystallization for PCM films. The calculated reflectivity contrast of Sb_2Te thin film is about 32%. A 10% threshold of optical contrast is necessary to maintain the minimum signal-to-noise ratio.[29] GeSb alloy is a prominent optical switching material that exhibits reflectivity contrast over 15%.[29] Multilevel reflectivity tunning of Sb_2Te_3 alloy has been proposed.[30] Nevertheless, little is known about the optical application of Sb_2Te thin film. This work demonstrates the potential of Sb_2Te thin film as a promising candidate for optical memory material. In the crystallization process, the resistance of Sb_2Te thin film drops obviously, while the reflectivity enhances significantly. Crystallization behavior determines the microstructure features that affect the optoelectronic properties, which need to be investigated.

Grain Growth

We have used EBSD to study the microstructure features of crystalline Sb_2Te thin film. Figure 3a displays the band contrast image of Sb_2Te thin film. The average grain size has been obtained, as shown in Fig. 3b. The average grain size is 0.329 ± 0.101 μm for Sb_2Te thin film annealed at 300°C, larger than that of $Ge_2Sb_2Te_5$ (~ 0.08 μm, annealed at 280°C),[31] suggesting the obvious grain growth tendency of Sb_2Te thin film. It is worth noting that the standard deviation of the average grain size is slightly large, implying grain inhomogeneity. We have calculated the grain size distribution, as shown in Fig. 3b. Grains with a diameter of 0.10–0.20 μm are predominantly present in the Sb_2Te thin film. Several grains with diameters ranging from 0.25 μm to 0.35 μm can be observed, displaying a broad range of grain

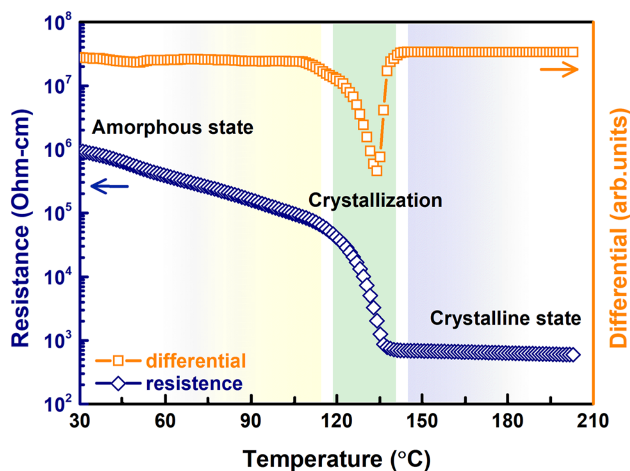

Fig. 1 Resistance–temperature curve of Sb_2Te thin film at a heating rate of 5°C min^{-1} and the calculated differential curve (top of panel).

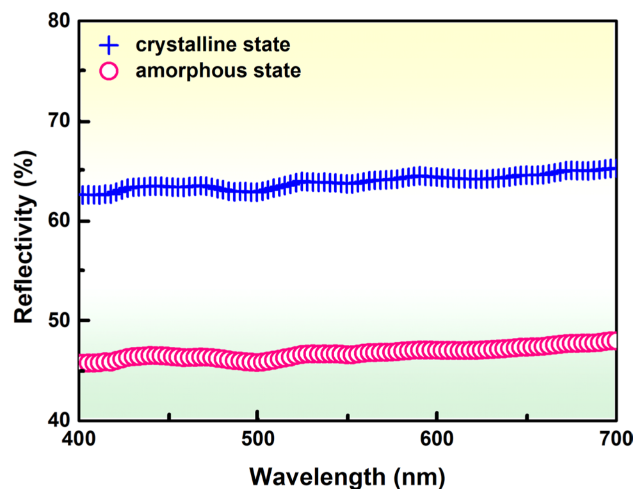

Fig. 2 Reflectivity versus wavelength curve for as-deposited and crystalline Sb_2Te thin films.

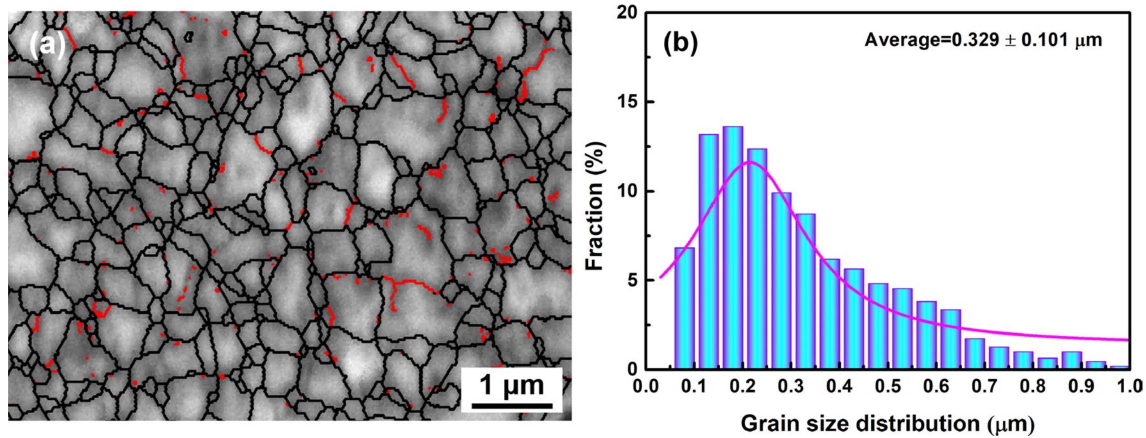

Fig. 3 (a) EBSD band contrast images of crystalline Sb_2Te thin film. The black lines indicate the high angle grain boundaries. The red lines denote the low-angle grain boundaries. (b) Grain size distribution and average grain size of crystalline Sb_2Te thin film (Color figure online).

sizes. Faster grain growth with limited nucleation rate causes differences in grain size of various nucleated areas.[32] Thus, inhomogeneous coarse grain may result from the strong crystallization tendency of Sb_2Te thin film, where the crystal growth controls the crystallization. The grain coarsening is accompanied by a decrease in the proportion of grain boundaries. The grain boundary shows stronger carrier and photon scattering.[33,34] Thus, the low ratio of grain boundaries is related to the increase of reflectivity and decrease of resistance. An in-depth understanding of the crystallization tendency and structure origin provides a reference for tuning microstructure and optoelectronic properties, which are discussed below.

Crystallization Kinetics of Sb_2Te Thin Film

Average Crystallization Activation Energy

We can obtain information on the crystallization features of Sb_2Te thin film by recording the DSC trace. Figure 4a shows the DSC curves for Sb_2Te thin films at various heating rates. The exothermic peak of the DSC curve indicates the crystallization of Sb_2Te thin film, which corresponds to the SET operation of the device, in which current pulses from sub-nanosecond to hundreds of nanoseconds are applied to crystallize the amorphous phase-change layer. Although heating speed of the DSC measurement employed in this work differs from the actual pulse rate, the kinetic parameters derived from the DSC traces at different heating rates can still provide insight into the crystallization behavior quantitatively. T_c is given by the exothermic peak position. The obtained T_cs at 10°C min^{-1}, 20°C min^{-1}, 30°C min^{-1}, and 40°C min^{-1} are 127.6°C, 132.7°C, 136.3°C, and 138.7°C, respectively. T_c values derived from DSC and R–T curves are agreement with each other. The crystallization activation energy (E_a) that is a crucial index to depict the difficulty of crystallization can be evaluated from the DSC curve by employing the Kissinger method. The Kissinger equation is as follows:[35]

$$\ln\left(\alpha/T_c^2\right) = C + \left(E_a/K_B T_c\right) \tag{2}$$

where α, C, and K_B are heating rate, constant, and Boltzmann constant, respectively. The plot of ln $(\alpha/T_c{}^2)$ versus $1/K_B T_c$ is shown in Fig. 4b. The average E_a, 1.82 eV, can be estimated from the slope of the linearly fitted line. The Kissinger relation can be simplified, which is as follows:[36]

$$\ln(\alpha) = C + \left(E_a/K_B T_c\right) \tag{3}$$

Figure 4c shows the fitting for ln (α) versus $1/K_B T_c$. The obtained average E_a is 1.88 eV, nearly equal to the value derived from Kissinger formula. The T_c and average E_a are sensitive to the experimental condition,[37] which is insufficient to understand the multi-step crystallization described by T_c and average E_a.

Local Crystallization Activation Energy

The local E_a that is also known as effective E_a corresponds to the amorphous structural evolution, which may be a more suitable parameter to qualify the thermal stability. To obtain the local E_a, we have calculated the crystallization fraction by first integrating the DSC traces. The crystallization fraction as a function of temperature is shown in Fig. 5a, where the typical S-shaped transition curves[38] can be observed. We can derive the local E_a by using Ozawa's method, which is as follows:[39]

$$\log(\alpha) = C - 0.4567\left(E_a/RT\right) \tag{4}$$

where R is the gas constant and T is the heating temperature. The curve of log (α) versus $1000/T$ is shown in Fig. 5b. The

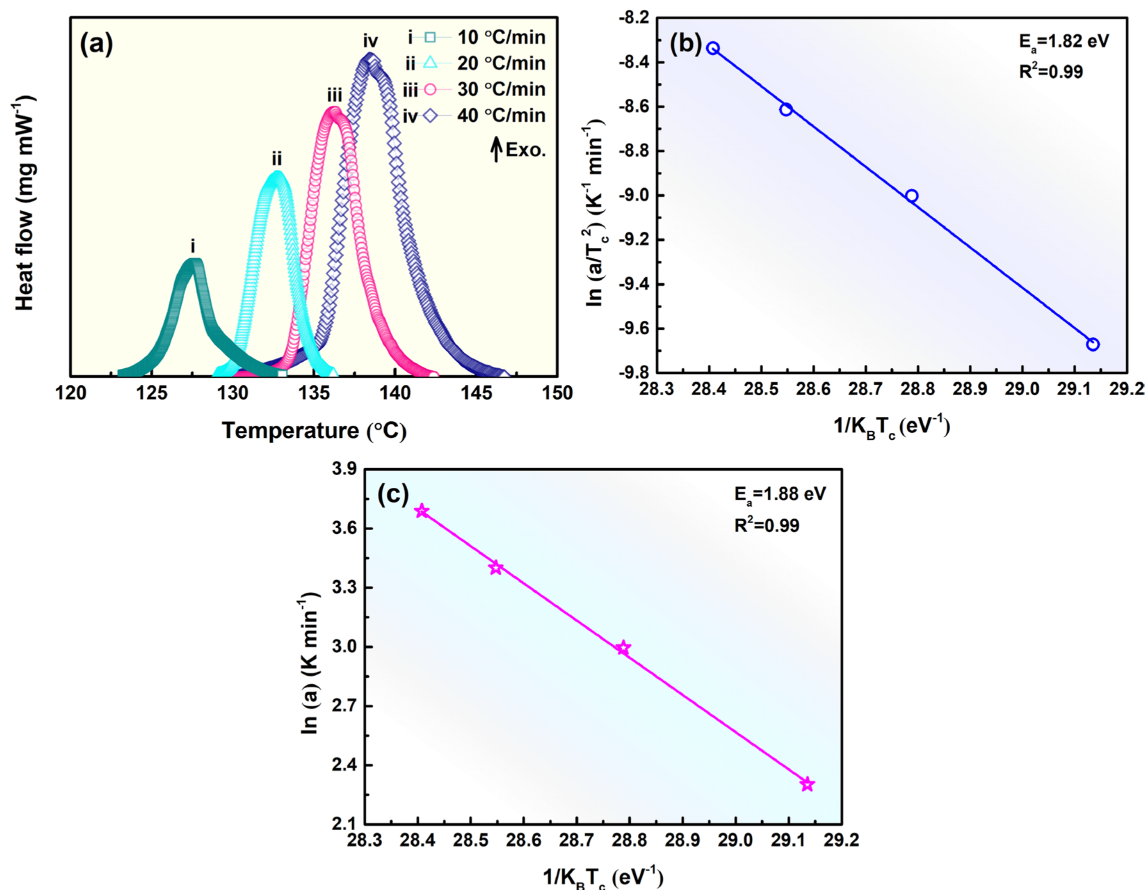

Fig. 4 (a) DSC curves for Sb_2Te thin films at different heating rates. (b) Plot of ln (α/T_c^2) versus $1/K_BT_c$ for average E_a calculation. (c) Plot of ln (α) versus $1/K_BT_c$ for average E_a calculation.

local E_a can be estimated from the slope of the linearly fitted lines. Figure 5c displays the local E_a as a function of crystallization fraction in the range of 0.1–0.9. The local E_a decreases continuously with increasing crystallization fraction, arising from an easier ordering of local bonding. The gradual saturation of nucleation and growth is accompanied by the decrease of local E_a.[3] 1.72 eV, the maximum value in Fig. 5c, is considered to be local E_a corresponding to the amorphous Sb_2Te thin film. The local E_a of Sb_2Te thin film is lower than that of $Ge_2Sb_2Te_5$ (~2.2 eV).[40] A stronger crystallization tendency of Sb_2Te thin film has been qualified by a lower local E_a and coarser grains. It may be accompanied with a higher crystal growth velocity, which is discussed in the following study.

Crystal Growth Velocity

Now, we turn to the discussion of fast crystal growth, which is one of the most important crystallization features of Sb_2Te. The crystal growth velocity (v) can be calculated by the following formula:

$$v = \frac{6D(T)}{\lambda}\left[1 - \exp\left(-\frac{\Delta G(T)}{K_B T}\right)\right] \tag{5}$$

where $D(T)$ is atomic diffusion coefficient, λ is average diffusion jumping distance (~0.1 nm),[41] and ΔG is Gibbs energy difference between amorphous and crystalline phases. In the crystallization process, atoms attach to the crystal nucleus at a certain rate. As temperature and composition fluctuate, atoms may become part of the stable nucleus. The gradual ordering of atomic arrangement results in the expansion of the crystal domain. Wilson[42] suggested that the rate and probability of atoms occupying lattice sites correspond to the atomic mobility and crystallization driving force. Accordingly, the coupling effect of atomic diffusion and driving force determines the crystal growth velocity, as shown in Eq. 5. Various models[43–46] have been developed to describe the growth velocity, where the driving force items are basically consistent with each other, while the kinetic coefficients in the diffusion term have been modified, which may yield different results. The Wilson method has been used to calculate the growth velocity of $Ag_4In_3Sb_{67}Te_{26}$,[5]

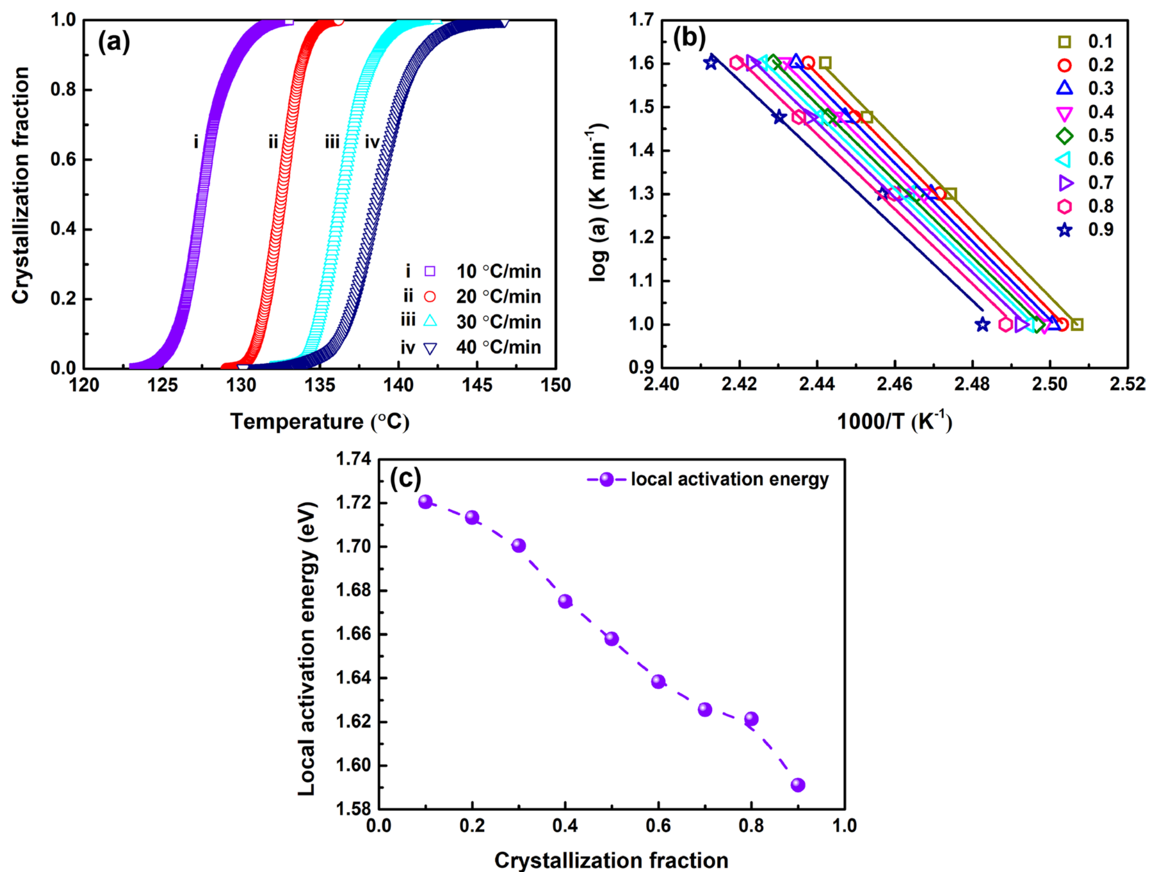

Fig. 5 (a) Crystallization fraction as a function of heating temperature at various heating rates. (b) Curve of log (α) versus 1000/T for calculation of local E_a. (c) Local E_a as a function of crystallization fraction in the range of 0.1 to 0.9.

which is utilized to describe the grain growth of Sb_2Te to provide a direct comparison.

The vital parameters (ΔG and D) are necessary to deduce the crystal growth velocity. The Gibbs energy difference can be calculated by Thompson-Spaepen[47] and Turnbull[48] approximations, as shown below:

$$\Delta G = \Delta H_m \frac{T_m - T}{T_m}\left(\frac{2T}{T_m + T}\right) \tag{6}$$

$$\Delta G = \Delta H_m \frac{\Delta T}{T} \tag{7}$$

where ΔH_m, T_m, and ΔT are melting enthalpy, melting temperature, and temperature difference, respectively. The melting enthalpy can be replaced by the crystallization enthalpy,[49] which derives from the DSC curve. Nevertheless, the heating rate may affect the exothermic signal of Sb_2Te thin film, causing a narrower exothermic peak, thus a smaller crystallization enthalpy. To calculate the Gibbs energy difference between amorphous and crystalline states, we have performed the DFT-MD to obtain the amorphous and crystalline models of Sb_2Te. Figure 6 displays the schematic diagram of the relaxed crystalline and amorphous structures. Figure 7 shows the obtained Gibbs energy difference between the relaxed amorphous and crystalline configurations. The calculated Gibbs energy differences of Sb[50] and $Ge_2Sb_2Te_5$[51] are also displayed. A smaller Gibbs energy difference implies a lower crystallization drive force, meaning the increased amorphous stability.[51] Although the Gibbs energy is tightly connected with the rapid crystallization, the atomic diffusion also plays a significant role on the crystallization and should be considered.

The mean square displacement (*MSD*) has been employed to describe the atomic mobility. A relatively lower temperature range (300–350 K) is chosen to observe the atomic diffusion behavior in stable amorphous state. Figure 8 shows the *MSD* of Sb, Te, and total atoms in amorphous Sb_2Te as a function of simulated time at different temperatures. All *MSD* curves are close to a straight line, which indicates that the atomic diffusion in the amorphous Sb_2Te tends to thermal equilibrium. Similar trace of amorphous PCM has been reported.[52] The motion of atoms in the steady state can

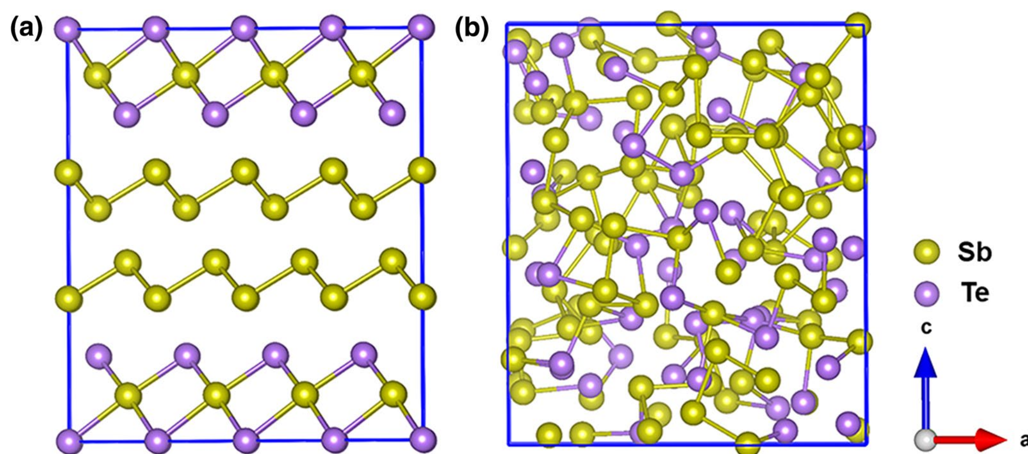

Fig. 6 Schematic diagram of the relaxed crystalline (a) and amorphous (b) structures. Sb and Te atoms are marked with dark yellow and light violet, respectively (Color figure online).

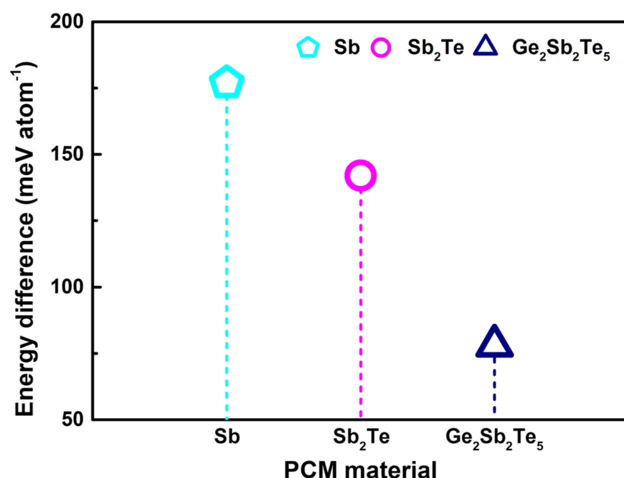

Fig. 7 Gibbs energy difference between amorphous and crystalline Sb_2Te, Sb ,[50] and $Ge_2Sb_2Te_5$[51] models. Data of Sb obtained by ab initio molecular dynamics simulation from Xu et al.[50] Data of $Ge_2Sb_2Te_5$ computed by ab initio calculation from Cho et al.[51]

be qualified by diffusion coefficient (D), which is calculated by the following equation:

$$D = \frac{1}{6}\frac{\partial}{\partial t}\lim_{t\to\infty} MSD. \tag{8}$$

Figure 8d shows the calculated diffusion coefficients of Sb, Te, and total atoms at 300 K, 325 K, and 350 K. The diffusion coefficient of total atoms in amorphous Sb_2Te is 1.19×10^{-11} m^2 s^{-1} at 300 K, close to the case in amorphous $Ge_{1.3}Bi_{0.5}Sb_{1.5}Te_3$ ($\sim2\times10^{-11}$ m^2 s^{-1}).[53] It is important to stress that Sb atoms are more diffusive than Te atoms, especially at higher temperatures. Sb atoms with strong mobility have also been observed in $Ge_{1.3}Bi_{0.5}Sb_{1.5}Te_3$[53] and $Ge_2Sb_2Te_5$,[8] which means that more Sb atoms promote the rapid phase transition, while Te atoms have an opposite effect.

The Gibbs energy difference and diffusion coefficient are used to calculate the crystal growth rate of Sb_2Te, as given in Table I. The grain growth velocity of Sb_2Te at 350 K (4.96 m s^{-1}) is higher than that of $Ag_4In_3Sb_{67}Te_{26}$[5] at 455 K (2.63 m s^{-1}) but close to that at 503 K (4.12 m s^{-1}), which confirms the rapid crystal growth of Sb_2Te. Current calculations may not accurately describe the non-Arrhenius behavior of the viscosity.[5] Nevertheless, knowledge of deduced crystal growth velocity could provide insights into the fast crystallization of PCM materials. Our results demonstrate the rapid crystal growth of Sb_2Te. Meanwhile, the visible inhibition effect of Ag and In on crystallization is revealed. Additionally, the grain growth is faster in Sb_2Te and $Ag_4In_3Sb_{67}Te_{26}$ than that in $Ge_2Sb_2Te_5$ (3 m s^{-1} at 650 K),[4] indicating the rapid crystallization of Sb-based PCM materials. Inhomogeneous and coarse grain, low crystallization activation energy, and high crystal growth velocity imply the strong crystallization tendency of Sb_2Te, whose structural origins should be explored. Furthermore, it is vital to survey the structural factors affecting the photoelectric conversion.

Local Structural Characteristics of Amorphous Sb_2Te Thin Film

Local Bonding Features of Amorphous Sb_2Te Thin Film

We have employed XPS to explore the bonding features of as-deposited Sb_2Te thin film. Figure 9a shows the XPS core level spectra of Sb 3d. The presence of Sb-Sb bonds in amorphous Sb_2Te thin film can be detected, whose binding energy peaks are located at 528.44 eV ($3d_{5/2}$) and 537.88 eV ($3d_{3/2}$). The binding energy of Sb $3d_{5/2}$ is close to that of O 1s, which may not facilitate in-depth discussion of the

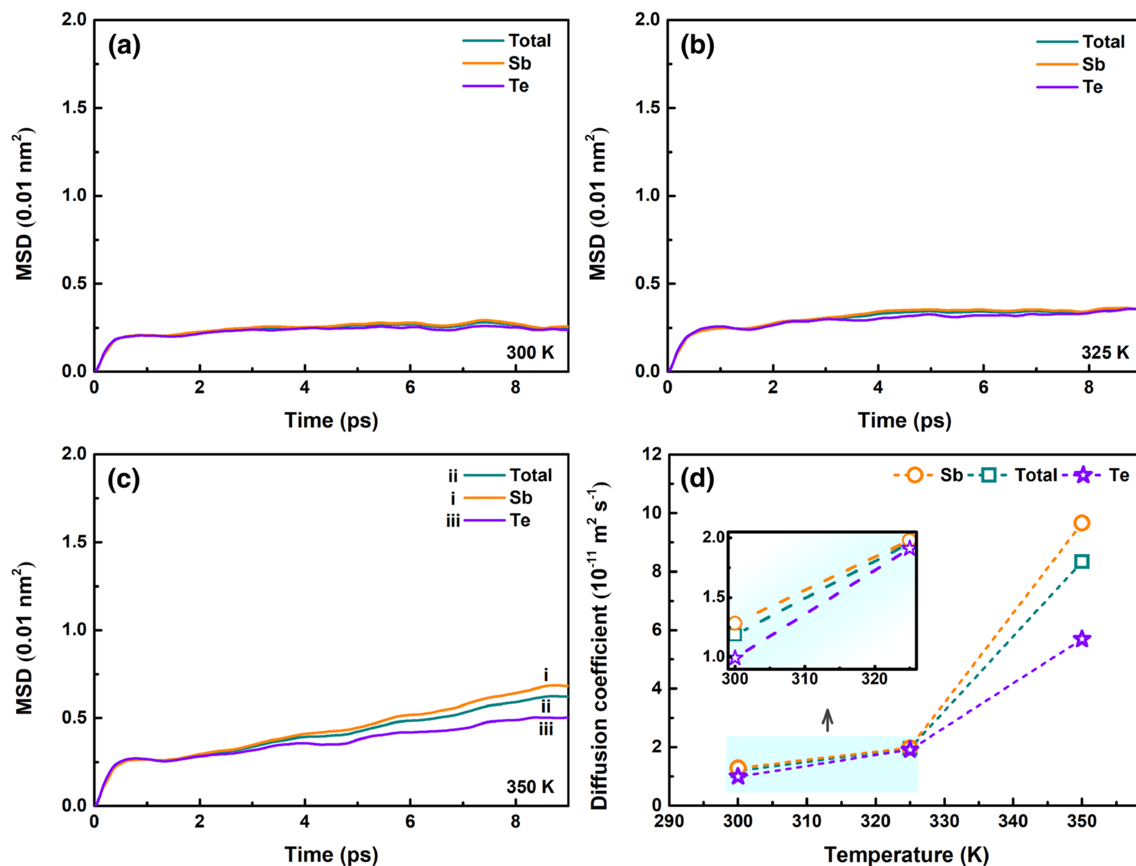

Fig. 8 *MSD* of Sb, Te, and total atoms in amorphous Sb_2Te as a function of simulated time at (a) 300 K, (b) 325 K, and (c) 350 K. (d) Diffusion coefficient of Sb, Te, and total atoms. The inset is an enlarged view of the diffusion coefficient in the range of 300 K to 325 K.

Table I Crystal growth velocity of Sb_2Te, $Ge_2Sb_2Te_5$,[4] and $Ag_4In_3Sb_{67}Te_{26}$,[5] data for $Ge_2Sb_2Te_5$ derived by ultrafast-heating calorimetry from Orava et al.,[4] data for $Ag_4In_3Sb_{67}Te_{26}$ computed by ab initio molecular dynamics simulation from Zhang et al.[5]

System	Sb_2Te	$Ge_2Sb_2Te_5$	$Ag_4In_3Sb_{67}Te_{26}$	
Growth velocity (m s^{-1})	4.96	3	2.63	4.12
Temperature (K)	350	650	455	503

bonding environment of Sb atoms. As reported in previous works,[16,22,54] the bonding of Sb to Te atoms has been clearly observed from the core level spectra of Sb 4*d* and Te 4*d*. We have analyzed the detailed spectra of Sb 4*d* and Te 4*d*, and recognized the significant Sb-Te binding energy peaks, as displayed in Fig. 9b, d. The dominance of Sb-Sb and Sb-Te bonds may constitute the matrix of amorphous Sb_2Te thin film. Te-Te homopolar bonds that should not be overlooked have been reported in amorphous PCM materials. As seen in Fig. 9c, the binding energy peaks of the Te 3*d* core level spectra appear at 572.55 eV (Te $3d_{5/2}$) and 582.94 eV (Te $3d_{3/2}$), confirming the formation of Te-Te bonds. As inferred from XPS measurements, the amorphous Sb_2Te thin film consists of Sb-Sb, Sb-Te, and Te-Te bonds.

We have examined the phonon vibration modes in the as-deposited Sb_2Te thin film by Raman spectroscopy. A broad flat Raman band ranging from 60 cm^{-1} to 220 cm^{-1} has been obtained, as shown in Fig. 10. This implies the disordered local environment of amorphous Sb_2Te thin film. A significant Raman characteristic peak occurs at ~ 150 cm^{-1}, corresponding to the contribution of Sb-Sb bonds (A_{1g}).[55] The vibrational modes at ~ 117 cm^{-1} (E_g) and ~ 169 cm^{-1} (A_{1g}) have also been observed, which are attributed to Sb-Te bonds.[56] The vibrating of Te-Te bonds (E_g) can be supported by the Raman peak at 92 cm^{-1}.[57] The information on the existence of Sb-O bonds has been displayed, and the slightly weaker vibrational mode is at ~ 197 cm^{-1}.[58] Raman studies show that Sb-Sb, Sb-Te, and Te-Te bonds are formed in amorphous Sb_2Te thin film, consistent with the results of XPS.

Local bonding in amorphous Sb_2Te is analyzed theoretically by using structure factor ($S(k)$). Last 3000 configurations in simulated quenching process have been used. We have calculated the pair correlation function ($g(r)$), which is a spherically averaged distribution of interatomic

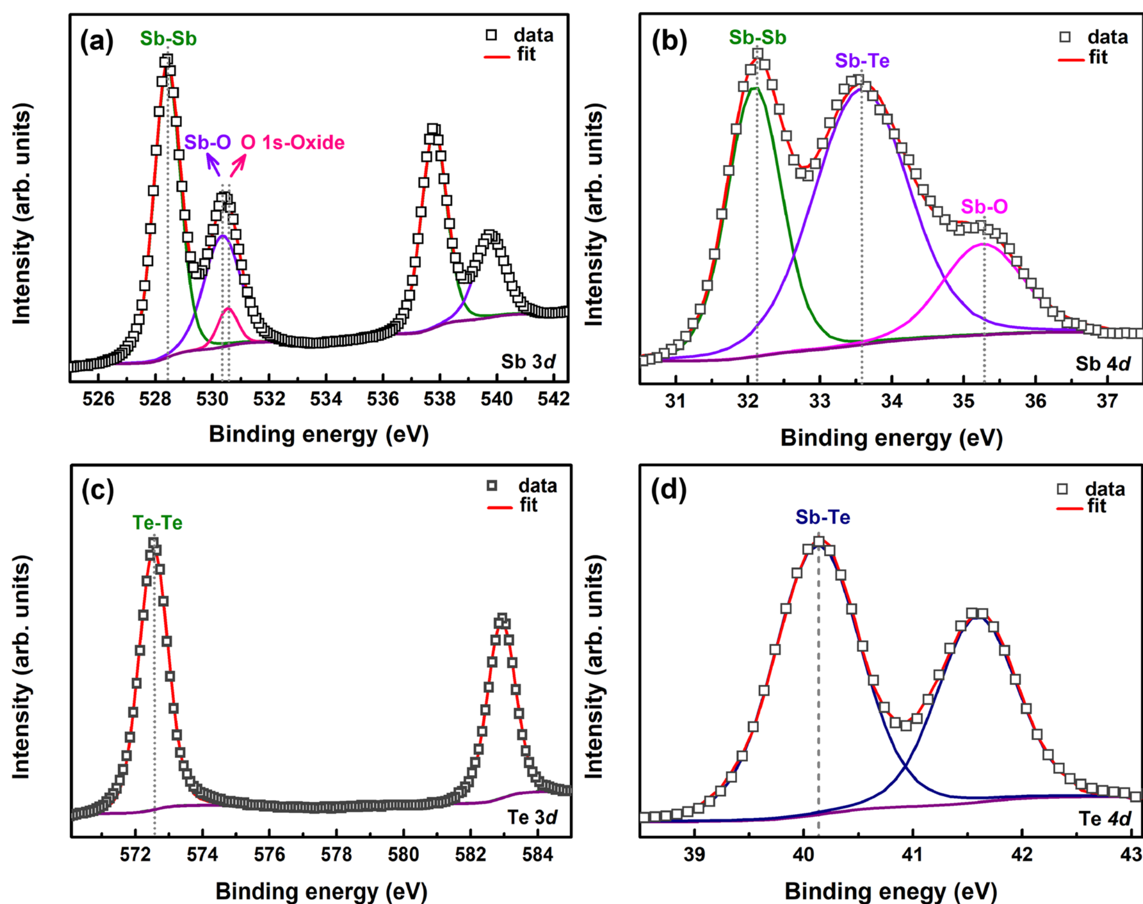

Fig. 9 XPS core level spectra of Sb 3*d* (a), Sb 4*d* (b), Te 3*d* (c), and Te 4*d* (d) for as-deposited Sb_2Te thin film.

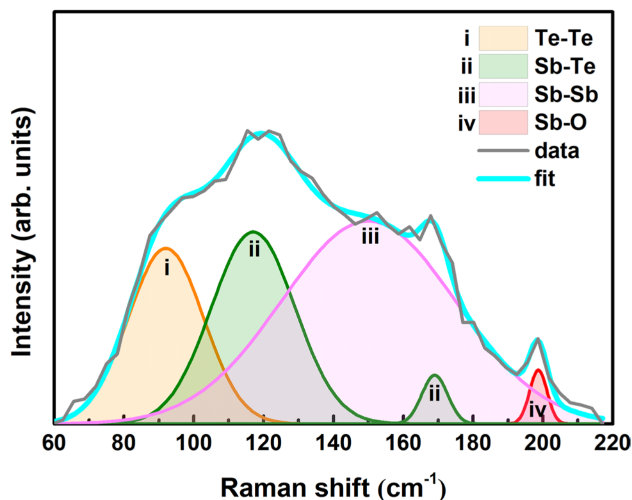

Fig. 10 Raman spectrum of as-deposited Sb_2Te thin film.

vectors. The S (k) can be obtained by Fourier transforming the (g (r)). The calculation details can be viewed in Caravati et al.[7] and Akola and Jones.[8] Figure 11 shows the obtained S (k)s. The main peak of total S (k) locates at 0.20 nm^{-1} with the intensity of 1.60 (Fig. 11a). Oscillations up to ~ 0.65 nm^{-1} can be observed for total S (k). As displayed in Fig. 11b, c, the decomposed partial S (k)s of Sb-Sb and Sb-Te pairs exhibit the strong peaks at ~ 0.20 nm^{-1}. The principal peak intensities of the decomposed partial S (k)s are 1.19 and 1.14 for Sb-Sb and Sb-Te pairs, respectively. The decomposed partial S (k) of Sb-Sb pair also contributes to the medium range order, including the second peak at 0.31 nm^{-1} and the third one at 0.43 nm^{-1}. It indicates the predominant contribution of Sb-Sb bonds. Simultaneously, numerous Sb-Te bonds are present. The weak peak of the decomposed partial S (k) is around 0.20 nm^{-1} for Te-Te pair (Fig. 10d), implying the existence of few Te-Te bonds. It is accepted that Sb atoms prefer to bond with Sb and Te atoms. The remaining Te atoms form chemical bonds with Te atoms. Therefore, amorphous Sb_2Te has large amount of homopolar bonds (considerable Sb-Sb bonds and several Te-Te bonds), as well as many heteropolar bonds (Sb-Te bonds). Although simulated quenching speed is different from the actual deposited rate, the formation of Sb-Sb, Sb-Te, and Te-Te

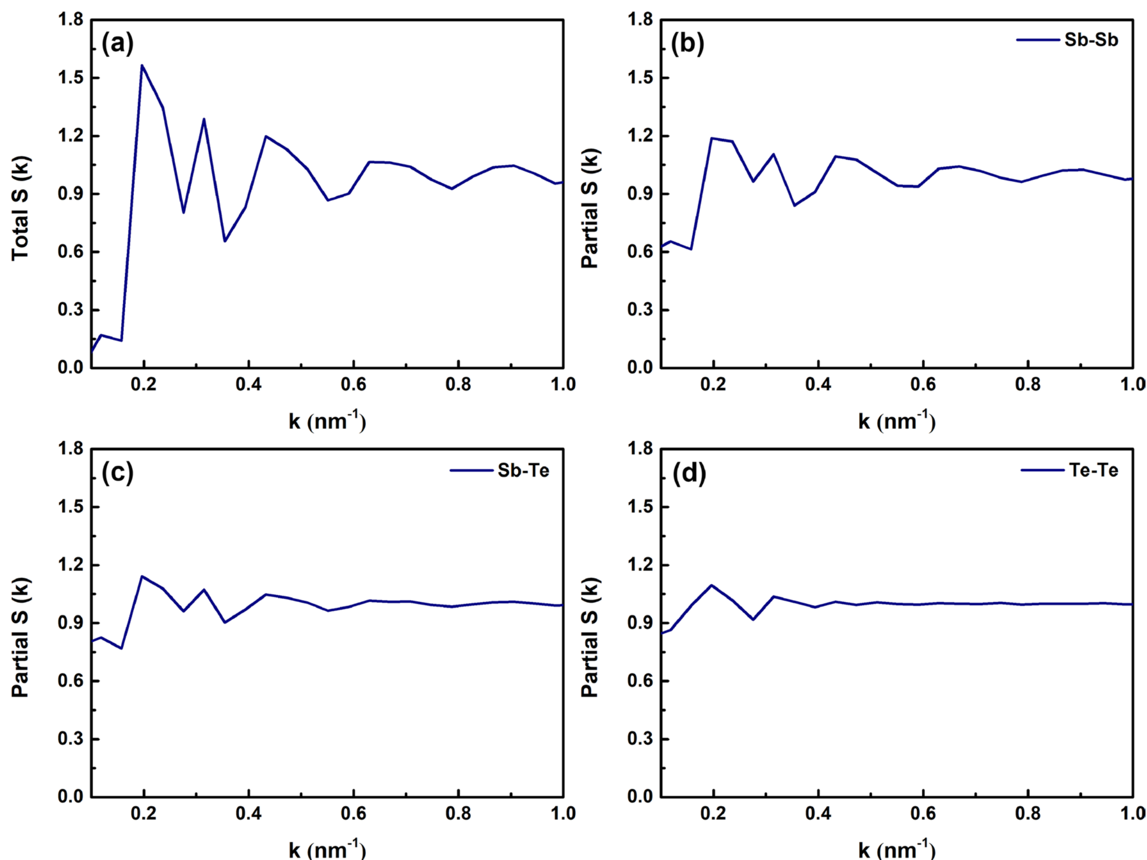

Fig. 11 Total (a) and decomposed partial structure factors of Sb-Sb pair (b), Sb-Te pair (c), and Te-Te pair (d) for amorphous Sb_2Te.

Table II Measured bond energy of Sb-Sb, Sb-Te, Te-Te, Ge-Ge, and Ge-Te bonds in crystalline state from Luo[59]

Chemical bond	Sb-Sb	Sb-Te	Te-Te	Ge-Ge	Ge-Te
Chemical bond energy (eV)	3.09	2.84	2.70	2.80	4.11

bonds in amorphous Sb_2Te can be supported by theoretical and experimental results.

Structural Origins of Higher Crystallization Tendency

The interaction and diffusion of atoms are the decisive factors in the crystallization process. Interactions between atoms can be characterized by the strength of chemical bonds. Nevertheless, the chemical bond length in the amorphous structure is not fixed. It is difficult to quantitatively calculate the strength of chemical bonds in the amorphous phase. Table II lists the measured bond energy of Sb-Sb, Sb-Te, and Te-Te bonds[59] in the crystalline state to provide an explanation. The information on Ge-Ge and Ge-Te bonds[59] is also given, which are the essential chemical bonds in amorphous $Ge_2Sb_2Te_5$. The bond energy of Sb-Sb and

Table III Calculated pre-exponential factor of diffusion (D_0) and activation energy of diffusion ($E_{diffusion}$) of total, Sb, and Te atoms for Sb_2Te

	Total	Sb	Te
D_0 (10^{-7} m^2 s^{-1})	1.79	1.87	1.53
$E_{diffusion}$ (eV)	0.35	0.36	0.31

Sb-Te bonds is much smaller than that of Ge-Te bonds. This may be an important structural origin that amorphous Sb_2Te has lower thermal stability than $Ge_2Sb_2Te_5$. The atomic mobility can be further discussed by calculating the pre-exponential diffusion factor (D_0) and diffusion activation energy ($E_{diffusion}$). The calculation equation is as follows:

$$D(T) = D_0 \exp\left(-\frac{E_{diffusion}}{k_B T}\right). \quad (9)$$

D(300 K), D(325 K), and D(350 K) are used. The obtained D_0 and $E_{diffusion}$ of total, Sb, and Te atoms are given in Table III. The calculated D_0 of Sb atoms (1.87×10^{-7} m^2 s^{-1}) is larger than that of Te atoms (1.53×10^{-7} m^2 s^{-1}), which

means that Sb atoms move faster than Te atoms, in agreement with the above result. Strong diffusion ability of Sb atoms may be another essential reason for the rapid crystallization of Sb_2Te.

Since the atomic geometry determines the crystallization mechanism, attention should be paid to the local structural primitives. It has been suggested that C atomic chains with C-C double bonds are formed in amorphous C-$Ge_2Sb_2Te_5$.[60] On the contrary, disordered C clusters were found in crystalline C-$Ge_2Sb_2Te_5$.[60] The two distinct configurations of C atoms increase the difference of local geometry before and after crystallization. The breaking of bonds and the diffusion of atoms become necessary processes for crystallization, which requires more activation energy and time. Consequently, crystallization is inhibited. In contrast, stable octahedral units induced by Sc atoms have been found in amorphous and crystalline Sb_2Te_3,[61] making the local bonding of two phases more similar. In the crystallization process, there are fewer broken chemical bonds and weaker atomic diffusion. Thus, the increase of local geometric similarity promotes rapid crystallization. As regards amorphous Sb_2Te, the Sb-centered octahedral bonding has been confirmed,[24] as occurs in the crystalline state. Therefore, we believe that octahedral unit is the main structural basis of high crystallization tendency, which makes the local geometry of the amorphous and crystalline phases more similar. Weaker chemical bonding and stronger atomic mobility further promote high-speed and low-activation-energy crystallization. Namely, the structural origins of strong crystallization tendency of Sb_2Te are local octahedral bonding, weak chemical bonds, and fast atomic movement.

Discussion on the Structural Factors of Optoelectronic Contrast

The role of amorphous local bonding on optoelectronic properties is also worth discussing. As stated in Caravati et al.[7] and Wełnic et al.,[62] the ratio of octahedron to tetrahedron changes enough to produce strong photoelectric transition, which means that differences in local geometry provide an optoelectronic contrast. The computational results showed that the variation of reflectivity results from the reduction of optical matrix elements in the amorphous phase, which is linked to the misalignment of the octahedron.[63] Sb_2Te exhibits local octahedral configuration. The misaligned octahedra decrease the medium range order of the amorphous phase, which is considered to be an important cause of optoelectronic difference. Numerous Sb-Sb bonds have been observed in amorphous Sb_2Te, which promotes the formation of Sb-centered nanoclusters.[64] The nanoclusters centered on Sb atoms change the motion path of carriers and photons and affect the photoelectric contrast. Furthermore, as previously mentioned, strong crystallization tendency coarsens the grains, which also plays a critical role in the optoelectronic properties.

Suggestion for More Stable Optoelectronic Memory Applications

In the present work, we have demonstrated the structural origins of higher crystallization tendency for Sb_2Te thin film. Local octahedral geometry with weak bonds and rapidly diffusing atoms is considered to be the major contributor. Moreover, we also discussed the structural factors of optoelectronic contrast for Sb_2Te thin film. Octahedral misalignment is believed to be the main cause. In order to achieve stable optoelectronic storage applications, the first step is to reduce the proportion of octahedral bonding in amorphous Sb_2Te to increase the structural contrast, which will improve the amorphous stability and support optoelectronic difference. It is also important to introduce the strong chemical bonds so that the structural rigidity can be enhanced and atomic diffusion can be dragged. The ameliorated crystallization tendency can also alter the microstructure characteristics and improve the optoelectronic properties.

Conclusions

We have investigated the crystallization behavior of Sb_2Te thin film to explore the potential as a sable photo-electronic memory material. The in situ resistance measurement results show that the resistance is reduced larger than 10^2 orders of magnitude in the crystallization process. The UV–Vis spectrum shows the optical reflectivity is increased by more than 30% before and after crystallization. The striking contrast meets the demands of optoelectronic storage applications. The deduced average crystallization activation energy is ~ 1.82 eV. The calculated local crystallization activation energy that corresponds to the amorphous state is 1.72 eV. The derived crystal growth velocity is 4.96 m s^{-1} at 350 K. The crystallization activation energy and crystal growth speed support the strong crystallization tendency of Sb_2Te thin film. The structural origins of photoelectric contrast and crystallization tendency have been discussed. The misaligned octahedrons promote the optoelectronic contrast. Moreover, the weak Sb-Sb, Sb-Te, and Te-Te bonds and fast-diffusing Sb atoms in octahedral geometry facilitate the low-activation-energy and high-speed crystallization. Therefore, it is believed that reducing the ratio of octahedral bonding and strengthening the chemical bonds could improve the crystallization properties of Sb_2Te thin film for more stable optoelectronic storage applications.

Acknowledgments The authors gratefully acknowledge the financial support of the National Natural Science Foundation of China (Grant No. 51771023).

Conflict of interest The authors declare that they have no conflict interest.

References

1. S.R. Ovshinsky, Reversible electrical switching phenomena in disordered structures. *Phys. Rev. Lett.* 21, 1450–1453 (1968). https://doi.org/10.1103/PhysRevLett.21.1450.
2. D. Lencer, M. Salinga, B. Grabowski, T. Hickel, J. Neugebauer, and M. Wuttig, A map for phase-change materials. *Nat. Mater.* 7, 972–977 (2008). https://doi.org/10.1038/nmat2330.
3. Y. Sutou, T. Kamada, M. Sumiya, Y. Saito, and J. Koike, Crystallization process and thermal stability of $Ge_1Cu_2Te_3$ amorphous thin films for use as phase change materials. *Acta Mater.* 60, 872–880 (2012). https://doi.org/10.1016/j.actamat.2011.10.048.
4. J. Orava, A.L. Greer, B. Gholipour, D.W. Hewak, and C.E. Smith, Characterization of supercooled liquid $Ge_2Sb_2Te_5$ and its crystallization by ultrafast-heating calorimetry. *Nat. Mater.* 11, 279–283 (2012). https://doi.org/10.1038/nmat3275.
5. W. Zhang, I. Ronneberger, P. Zalden, M. Xu, M. Salinga, M. Wuttig, and R. Mazzarello, How fragility makes phase-change data storage robust: insights from ab initio simulations. *Sci. Rep.* 4, 6529 (2014). https://doi.org/10.1038/srep06529.
6. A.V. Kolobov, P. Fons, A.I. Frenkel, A.I. Ankudinov, J. Tominaga, and T. Uruga, Understanding the phase-change mechanism of rewritable optical media. *Nat. Mater.* 3, 703–708 (2004). https://doi.org/10.1038/nmat1215.
7. S. Caravati, M. Bernasconi, T.D. Kühne, M. Krack, and M. Parrinello, Coexistence of tetrahedral- and octahedral-like sites in amorphous phase change materials. *Appl. Phys. Lett.* 91, 171906 (2007). https://doi.org/10.1063/1.2801626.
8. J. Akola and R.O. Jones, Structural phase transitions on the nanoscale: the crucial pattern in the phase-change materials $Ge_2Sb_2Te_5$ and GeTe. *Phys. Rev. B* 76, 235201 (2007). https://doi.org/10.1103/PhysRevB.76.235201.
9. G.Y. Liu, L.C. Wu, M. Zhu, Z.T. Song, F. Rao, S.N. Song, and Y. Cheng, The investigations of characteristics of Sb_2Te as a base phase-change material. *Solid-State Electron.* 135, 31–36 (2017). https://doi.org/10.1016/j.sse.2017.06.004.
10. Y. Wang, T.Q. Guo, G.Y. Liu, T. Li, S.L. Lv, S.N. Song, Y. Cheng, W.X. Song, K. Ren, and Z.T. Song, Sc-centered octahedron enables high-speed phase change memory with improved data retention and reduced power consumption. *ACS Appl. Mater. Interfaces* 11, 10848–10855 (2019). https://doi.org/10.1021/acsami.8b22580.
11. L.Y. Peng, Z. Li, G.J. Wang, J. Zhou, R. Mazzarello, and Z.M. Sun, Reduction in thermal conductivity of Sb_2Te phase-change material by scandium/yttrium doping. *J. Alloys Compd.* 821, 153499 (2020). https://doi.org/10.1016/j.jallcom.2019.153499.
12. J.S. Zhao, Q. Liang, Y. Chen, S.F. Zhang, Z.T. Song, S.N. Song, Z.Y. Ma, and L.C. Wu, Rhenium doped Sb_2Te phase change material with ultrahigh thermal stability and high speed. *J. Alloys Compd.* 863, 158583 (2021). https://doi.org/10.1016/j.jallcom.2020.158583.
13. Y. Xue, S. Yan, S.L. Lv, and Z.T. Song, Ta-doped Sb_2Te allows ultrafast phase-change memory with excellent high-temperature operation characteristics. *Nano-Micro Lett.* 13, 33 (2021). https://doi.org/10.1007/s40820-020-00557-4.
14. X. Chen, Y.H. Zheng, M. Zhu, K. Ren, Y. Wang, T. Li, G.Y. Liu, T.Q. Guo, L. Wu, X.Q. Liu, Y. Cheng, and Z.T. Song, Scandium doping brings speed improvement in Sb_2Te alloy for phase change random access memory application. *Sci. Rep.* 8, 6839 (2018). https://doi.org/10.1038/s41598-018-25215-z.
15. G.X. Wang, X. Shen, Q.H. Nie, H. Wang, Y.G. Lu, and D.T. Shi, Improved thermal stability of C-doped Sb_2Te films by increasing degree of disorder for memory application. *Thin Solid Films* 615, 345–350 (2016). https://doi.org/10.1016/j.tsf.2016.07.059.
16. Y.H. Zheng, Y. Cheng, M. Zhu, X.L. Ji, Q. Wang, S.N. Song, Z.T. Song, W.L. Liu, and S.L. Feng, A candidate Zr-doped Sb_2Te alloy for phase change memory application. *Appl. Phys. Lett.* 108, 052107 (2016). https://doi.org/10.1063/1.4941418.
17. L. Kang and L. Chen, Overview of the role of alloying modifiers on the performance of phase change memory materials. *J. Electron. Mater.* 50, 1–24 (2021). https://doi.org/10.1007/s11664-020-08590-0.
18. H. Wang, G.X. Wang, Y.M. Chen, X. Shen, Y.G. Lv, and Q.H. Nie, Advantages of $Mo_{4.9}(Sb_2Te)_{95.1}$ film with improved crystallization properties for phase change memory. *Mater. Lett.* 161, 240–243 (2015). https://doi.org/10.1016/j.matlet.2015.08.109.
19. X. Shen, G.X. Wang, P.R. Wang, S.X. Dai, L.C. Wu, Y.M. Chen, T.F. Xu, and Q.H. Nie, Enhanced thermal stability and electrical behavior of Zn-doped Sb_2Te films for phase change memory application. *Appl. Phys. Lett.* 102, 131902 (2013). https://doi.org/10.1063/1.4799370.
20. Y.F. Gu, S.N. Song, Z.T. Song, S.Y. Bai, Y. Cheng, Z.H. Zhang, B. Liu, and S.L. Feng, Phase-change material $Ge_{0.61}Sb_2Te$ for application in high-speed phase change random access memory. *Appl. Phys. Lett.* 102, 103110 (2013). https://doi.org/10.1063/1.4795595.
21. Y.G. Lu, S.N. Song, Z.T. Song, F. Rao, L.C. Wu, M. Zhu, B. Liu, and D.N. Yao, Investigation of $CuSb_4Te_2$ alloy for high-speed phase change random access memory applications. *Appl. Phys. Lett.* 100, 193114 (2012). https://doi.org/10.1063/1.4711811.
22. M. Zhu, L.C. Wu, Z.T. Song, F. Rao, D.L. Cai, C. Peng, X.L. Zhou, K. Ren, S.N. Song, B. Liu, and S.L. Feng, $Ti_{10}Sb_{60}Te_{30}$ for phase change memory with high-temperature data retention and rapid crystallization speed. *Appl. Phys. Lett.* 100, 122101 (2012). https://doi.org/10.1063/1.3695036.
23. C. Peng, L.C. Wu, F. Rao, Z.T. Song, P.X. Yang, H.J. Song, K. Ren, X.L. Zhou, M. Zhu, B. Liu, and J.H. Chu, W-Sb-Te phase-change material: a candidate for the trade-off between programming speed and data retention. *Appl. Phys. Lett.* 101, 122108 (2012). https://doi.org/10.1063/1.4754138.
24. W. Zhang, I. Ronneberger, Y. Li, and R. Mazzarello, Ab initio investigation of amorphous Sb_2Te. *Monatsh. Chem.* 145, 97–101 (2014). https://doi.org/10.1007/s00706-013-0980-0.
25. M.D. Segall, P.J.D. Lindan, M.J. Probert, C.J. Pickard, P.J. Hasnip, S.J. Clark, and M.C. Payne, First-principles simulation: ideas, illustrations and the CASTEP code. *J. Phys. Condens. Matter* 14, 2717–2744 (2002). https://doi.org/10.1088/0953-8984/14/11/301.
26. J.P. Perdew, K. Burke, and M. Ernzerhof, Generalized gradient approximation made simple. *Phys. Rev. Lett.* 77, 3865–3868 (1996). https://doi.org/10.1103/PhysRevLett.77.3865.
27. R.E. Simpson, M. Krbal, P. Fons, A.V. Kolobov, J. Tominaga, T. Uruga, and H. Tanida, Toward the ultimate limit of phase change in $Ge_2Sb_2Te_5$. *Nano Lett.* 10, 414–419 (2010). https://doi.org/10.1021/nl902777z.
28. G. Bakan, B. Gerislioglu, F. Dirisaglik, Z. Jurado, L. Sullivan, A. Dana, C. Lam, A. Gokirmak, and H. Silva, Extracting the temperature distribution on a phase-change memory cell during crystallization. *J. Appl. Phys.* 120, 164504 (2016). https://doi.org/10.1063/1.4966168.
29. C.C. Liu, X.R. Cao, J. Wang, Y.F. Yuan, J. Su, C.M. Liu, L. Cheng, X.T. Zhang, J. Li, and X. Zhang, Investigation on the optical phase change properties of intrinsic GeSb and Ti-doped

GeSb. *Opt. Mater. Express* 8, 936–947 (2018). https://doi.org/10.1364/OME.8.000936.
30. Y. Meng, J.K. Behera, Z.W. Wang, J.L. Zheng, J.S. Wei, L.C. Wu, and Y. Wang, Nanostructure patterning of C-Sb_2Te_3 by maskless thermal lithography using femtosecond laser pulses. *Appl. Surf. Sci.* 508, 145228 (2020). https://doi.org/10.1016/j.apsusc.2019.145228.
31. D.Z. Dimitrov, Y.H. Lu, M.R. Tseng, W.C. Hsu, and H.P.D. Shien, Oxygen and nitrogen Co-doped GeSbTe thin films for phase-change optical recording. *Jpn. J. Appl. Phys.* 41, 1656–1659 (2002). https://doi.org/10.1143/JJAP.41.1656.
32. G. Eising, B.J. Niebuur, A. Pauza, and B.J. Kooi, Competing crystal growth in Ge-Sb phase-change films. *Adv. Funct. Mater.* 24, 1687–1694 (2014). https://doi.org/10.1002/adfm.201301242.
33. K.S. Bang, Y.J. Oh, and S.Y. Lee, Effect of InP doping on the phase transition of thin GeSbTe films. *J. Electron. Mater.* 44, 2712–2718 (2015). https://doi.org/10.1007/s11664-015-3734-4.
34. I.N. Chen, C.W. Chong, D.P. Wong, L.M. Lyu, W.L. Chien, R. Anbalagan, M. Aminzare, Y.F. Chen, L.C. Chen, and K.H. Chen, Improving the thermoelectric performance of metastable rock-salt GeTe-rich Ge-Sb-Te thin films through tuning of grain orientation and vacancies. *Phys. Status Solidi A* 213, 3122–3129 (2016). https://doi.org/10.1002/pssa.201600274.
35. H.E. Kissinger, Reaction kinetics in differential thermal analysis. *Anal. Chem.* 29, 1702–1706 (1957). https://doi.org/10.1021/ac60131a045.
36. S. Mahadevan, A. Giridhar, and A.K. Singh, Calorimetric measurements on As-Sb-Se glasses. *J. Non-Cryst. Solids* 88, 11–34 (1986). https://doi.org/10.1016/S0022-3093(86)80084-9.
37. A.H. Moharram, A.A. Abu-sehly, M.A. El-Oyoun, and A. Soltan, Pre-crystallization and crystallization kinetics of some Se-Te-Sb glasses. *Phys. B* 324, 344–351 (2002). https://doi.org/10.1016/S0921-4526(02)01421-7.
38. Y.C. Her and Y.S. Hsu, Thickness dependence of crystallization and melting kinetics of eutectic $Sb_{70}Te_{30}$ phase change recording film. *J. Non-Cryst. Solids* 354, 3129–3134 (2008). https://doi.org/10.1016/j.jnoncrysol.2008.01.021.
39. T. Ozawa, Kinetic analysis of derivative curves in thermal analysis. *J. Therm. Anal.* 2, 301–324 (1970). https://doi.org/10.1007/bf01911411.
40. A. Sherchenkov, S. Kozyukhin, A. Babich, and P. Lazarenko, Thermal properties of phase change material $Ge_2Sb_2Te_5$ doped with Bi. *J. Non-Cryst. Solids* 377, 26–29 (2013). https://doi.org/10.1016/j.jnoncrysol.2013.01.006.
41. M. Salinga, E. Carria, A. Kaldenbach, M. Bornho, J. Benke, J. Mayer, and M. Wuttig, Measurement of crystal growth velocity in a melt-quenched phase-change material. *Nat. Commun.* 4, 2371 (2013). https://doi.org/10.1038/ncomms3371.
42. H.A. Wilson, On the velocity of solidification and viscosity of super-cooled liquids. *Philos. Mag.* 50, 238–250 (1900). https://doi.org/10.1080/14786440009463908.
43. J. Barták, P. Košťál, and J. Málek, Analysis of crystal growth and viscosity in Ge-Sb-Se-Te undercooled melts. *J. Non-Cryst. Solids* 505, 1–8 (2019). https://doi.org/10.1016/j.jnoncrysol.2018.10.048.
44. M.H. Cohen and G.S. Grest, Liquid-glass transition, a free-volume approach. *Phys. Rev. B* 20, 1077–1098 (1979). https://doi.org/10.1103/PhysRevB.20.1077.
45. J.C. Mauro, Y.Z. Yue, A.J. Ellison, P.K. Gupta, and D.C. Allan, Viscosity of glass-forming liquids. *Proc. Natl. Acad. Sci. U. S. A.* 106, 19780–19784 (2009). https://doi.org/10.1073/pnas.091170510.
46. J. Orava, D.W. Hewak, and A.L. Greer, Fragile-to-strong crossover in supercooled liquid Ag-In-Sb-Te studied by ultrafast calorimetry. *Adv. Funct. Mater.* 25, 4851–4858 (2015). https://doi.org/10.1002/adfm.201501607.
47. C.V. Thompson and F. Spaepen, Approximation of the free-energy change on crystallization. *Acta Metall.* 27, 1855–1859 (1979). https://doi.org/10.1016/0001-6160(79)90076-2.
48. D. Turnbull, Formation of crystal nuclei in liquid metals. *J. Appl. Phys.* 21, 1022–1028 (1950). https://doi.org/10.1063/1.1699435.
49. J. Barták, P. Košťál, V. Podzemná, J. Shánělová, and J. Málek, Crystal growth kinetics and viscous behavior in $Ge_2Sb_2Se_5$ undercooled melt. *J. Phys. Chem. B* 120, 7998–8006 (2016). https://doi.org/10.1021/acs.jpcb.6b05455.
50. M. Xu, B.W. Li, K.L. Xu, H. Tong, X.M. Cheng, M. Xu, and X.S. Miao, Stabilizing amorphous Sb by adding alien seeds for durable memory materials. *Phys. Chem. Chem. Phys.* 21, 4494–4500 (2019). https://doi.org/10.1039/C8CP07446A.
51. E. Cho, S. Han, D. Kim, H. Horii, and H.S. Nam, Ab initio study on influence of dopants on crystalline and amorphous $Ge_2Sb_2Te_5$. *J. Appl. Phys.* 109, 043705 (2011). https://doi.org/10.1063/1.3553851.
52. L.C. Zhang, B.S. Sa, J. Zhou, Z.T. Song, and Z.M. Sun, Atomic scale insight into the amorphous structure of Cu doped GeTe phase-change material. *J. Appl. Phys.* 116, 153501 (2014). https://doi.org/10.1063/1.4898074.
53. K. Ren, Y. Wang, S.L. Lv, S.S. Zhu, T.J. Xin, and Z.T. Song, Reducing structural change in the phase transition of Ge-doped $Bi_{0.5}Sb_{1.5}Te_3$ to enable high-speed and low-energy memory switching. *J. Mater. Chem. C* 7, 11813–11823 (2019). https://doi.org/10.1039/C9TC03494C.
54. S. Sahu, A. Manivannan, H. Shaik, and G.M. Rao, Local structure of amorphous $Ag_5In_5Sb_{60}Te_{30}$ and In_3SbTe_2 phase change materials revealed by X-ray photoelectron and Raman spectroscopic studies. *J. Appl. Phys.* 122, 015305 (2017). https://doi.org/10.1063/1.4991491.
55. R. Hunger, N. Blick, N. Esser, M. Arens, W. Richter, V. Wagner, and J. Geurts, Growth of Sb on Si (111) studied by Raman scattering. *Surf. Sci.* 307–309, 1061–1065 (1994). https://doi.org/10.1016/0039-6028(94)91540-7.
56. Y. Kim, X. Chen, Z. Wang, J. Shi, I. Miotkowski, Y.P. Chen, P.A. Sharma, A.L. Lima Sharma, M.A. Hekmaty, Z. Jiang, and D. Smirnov, Temperature dependence of Raman-active optical phonons in Bi_2Se_3 and Sb_2Te_3. *Appl. Phys. Lett.* 100, 071907 (2012). https://doi.org/10.1063/1.3685465.
57. P.M. Amirtharaj and F.H. Pollak, Raman scattering study of the properties and removal of excess Te on CdTe surfaces. *Appl. Phys. Lett.* 45, 789–791 (1984). https://doi.org/10.1063/1.95367.
58. S.J. Gilliam, J.O. Jensen, A. Banerjee, D. Zeroka, S.J. Kirkby, and C.N. Merrow, A theoretical and experimental study of Sb_4O_6: vibrational analysis, infrared, and Raman spectra. *Spectrochim. Acta Part A* 60, 425–434 (2004). https://doi.org/10.1016/S1386-1425(03)00245-2.
59. Y.R. Luo, *Experimental Data of Chemical Bond Energies* (Beijing: Science Press, 2005).
60. X.L. Zhou, M.J. Xia, F. Rao, L.C. Wu, X.B. Li, Z.T. Song, S.L. Feng, and H.B. Sun, Understanding phase-change behaviors of carbon-doped $Ge_2Sb_2Te_5$ for phase-change memory application. *ACS Appl. Mater. Interfaces* 6, 14207–14214 (2014). https://doi.org/10.1021/am503502q.
61. F. Rao, K.Y. Ding, Y.X. Zhou, Y.H. Zheng, M.J. Xia, S.L. Lv, Z.T. Song, S.L. Feng, I. Ronneberger, R. Mazzarello, W. Zhang, and E. Ma, Reducing the stochasticity of crystal nucleation to enable subnanosecond memory writing. *Science* 358, 1423–1427 (2017). https://doi.org/10.1126/science.aao3212.
62. W. Wełnic, S. Botti, L. Reining, and M. Wuttig, Origin of the optical contrast in phase-change materials. *Phys. Rev. Lett.* 98, 236403 (2007). https://doi.org/10.1103/PhysRevLett.98.236403.
63. S. Ahmed, X.D. Wang, Y.X. Zhou, L. Sun, R. Mazzarello, and W. Zhang, Unraveling the optical contrast in Sb_2Te and AgInSbTe

phase-change materials. *J. Phys. Photonics* 3, 034011 (2021). https://doi.org/10.1088/2515-7647/ac051b.

64. J. Kalikka, J. Akola, and R.O. Jones, Density functional simulations of structure and polymorphism in Ga/Sb films. *J. Phys. Condens. Matter* 25, 115801 (2013). https://doi.org/10.1088/0953-8984/25/11/115801.

Publisher's Note Springer Nature remains neutral with regard to jurisdictional claims in published maps and institutional affiliations.

Springer Nature or its licensor (e.g. a society or other partner) holds exclusive rights to this article under a publishing agreement with the author(s) or other rightsholder(s); author self-archiving of the accepted manuscript version of this article is solely governed by the terms of such publishing agreement and applicable law.